Title: Structure-Function Dissociations of Human Hippocampal Subfield Stiffness and Memory Performance

Abbreviated Title: Hippocampal Subfield Stiffness and Memory Function

Peyton L Delgorio[1], Lucy V Hiscox[1], Ana M Daugherty[2], Faria Sanjana[3], Grace McIlvain[1], Ryan T Pohlig[4], Matthew DJ McGarry[5], Christopher R Martens[3], Hillary Schwarb[6], Curtis L Johnson[1]

1 Department of Biomedical Engineering, University of Delaware, Newark, DE, 19716, USA

2 Department of Psychology and Institute of Gerontology, Wayne State University, Detroit, MI, 48202, USA

3 Department of Kinesiology and Applied Physiology, University of Delaware, Newark, DE, 19713, USA

4 Biostatistics Core Facility, College of Health Sciences, University of Delaware, Newark, DE, 19716, USA

5 Thayer School of Engineering, Dartmouth College, Hanover, NH, 03755, USA

6 Beckman Institute for Advanced Science and Technology, University of Illinois at Urbana-Champaign, Urbana, IL, 61801, USA

Correspondence to: Curtis L Johnson, clj@udel.edu

Text Pages: 34

Figures: 6

Tables: 6

Words: **Abstract:** 240
Introduction: 648
Discussion: 1498

Financial Interests or Conflicts of Interest: We have no financial interests or conflicts of interest to disclose.

Acknowledgements: This research was supported by grants from the National Institutes of Health (R01-AG058853, R01-EB027577, K01-AG054731, and R03-AG065894), Delaware INBRE (P20-GM103446), Delaware Cardiovascular COBRE (P20-GM113125), and Delaware Neuroscience COBRE (P20-GM103653).

Abstract

Aging and neurodegenerative diseases lead to decline in thinking and memory ability. The subfields of the hippocampus (HCsf) play important roles in memory formation and recall. Imaging techniques sensitive to the underlying HCsf tissue microstructure can reveal unique structure-function associations and their vulnerability in aging and disease. The goal of this study was to use magnetic resonance elastography (MRE), a noninvasive MR imaging-based technique that can quantitatively image the viscoelastic mechanical properties of tissue, to determine the associations of HCsf stiffness with different cognitive domains across the lifespan. 88 adult participants completed the study (age: 23-81 years, M/F 36/51), in which we aimed to determine which HCsf regions most strongly correlated with different memory performance outcomes and if viscoelasticity of specific HCsf regions mediated the relationship between age and performance. Our results revealed that both interference cost on a verbal memory task and relational memory task performance were significantly related to cornu ammonis 1-2 (CA1-CA2) stiffness ($p = 0.018$ and $p = 0.011$, respectively), with CA1-CA2 stiffness significantly mediating the relationship between age and interference cost performance ($p = 0.031$). There were also significant associations between delayed free verbal recall performance and stiffness of both the dentate gyrus-cornu ammonis 3 (DG-CA3) ($p = 0.016$) and subiculum (SUB) ($p = 0.032$) regions. This further exemplifies the functional specialization of HCsf in declarative memory and the potential use of MRE measures as clinical biomarkers in assessing brain health in aging and disease.

Significance Statement

Hippocampal subfields are cytoarchitecturally-unique structures involved in distinct aspects of memory processing. Magnetic resonance elastography is a technique that can noninvasively image tissue viscoelastic mechanical properties, potentially serving as sensitive biomarkers of aging and neurodegeneration related to functional outcomes. High-resolution *in vivo* imaging has invigorated interest in determining subfield functional specialization and their differential vulnerability in aging and disease. Applying MRE to probe subfield-specific cognitive correlates will indicate that measures of subfield stiffness can determine the integrity of structures supporting specific domains of memory performance. These findings will further validate our high-resolution MRE method and support the potential use of subfield stiffness measures as clinical biomarkers in classifying aging and disease states.

Introduction

The hippocampus (HC) is a brain structure involved in memory formation and demonstrates structural decline in aging and neurodegenerative disease, such as Alzheimer's disease (Morrison and Hof, 1997; Petersen et al., 2000). The individual subfields of the HC (HCsf) (Duvernoy, 2005) include the dentate gyrus (DG), cornu ammonis sectors 1-3 (CA1-3), and subiculum (SUB), which function together to retrieve, encode, and process memory (de Flores et al., 2015). *In vivo* human imaging studies suggest the HCsf follow different trajectories of decline in age and related disease, plausibly due to a differential decrease in neuron density and myelin sheath degradation (West, 1993; Wisse et al., 2014; Daugherty et al., 2016). Advanced age correlates with smaller HCsf volumes, and partially accounts for age-related memory deficits in a region-specific manner as the HCsf each support distinct memory functions (Mueller et al., 2007, 2011; Daugherty et al., 2016; Zammit et al., 2017). Whereas DG and CA3 correlate with relational memory performance, CA1 correlates with comparing current experience to episodic recollection, while SUB is suggested to support memory integration and delayed recall (Golomb et al., 1996; Leal and Yassa, 2018; Foster et al., 2019; Radhakrishnan et al., 2020). However, evidence of specific structural correlates to memory function using gross volumetric or diffusion MRI-based estimates leaves an open question of the underlying changes in tissue microstructure. Imaging techniques sensitive to individual HCsf tissue integrity have the potential to contribute to scientific understanding of the degeneration of these regions with age and mechanisms of memory decline.

Magnetic resonance elastography (MRE) is a sensitive neuroimaging modality that can provide reliable estimates of tissue viscoelastic mechanical properties (Hiscox et al., 2016). MRE studies have shown changes in brain tissue viscoelasticity with aging (Hiscox et al., 2021) and in neurodegenerative diseases (Murphy et al., 2019). Alterations in these properties are thought to reflect biological changes in the microstructural composition and organization of the tissue (Sack et al., 2013). Our group has previously observed strong relationships between HC viscoelasticity and memory task performance in both young and older adults (Schwarb et al., 2016; Hiscox et al., 2018), further highlighting that MRE metrics are functionally relevant, may provide insight into memory performance decline across the lifespan, and are potential clinical biomarkers of cognitive aging.

We recently developed a high-resolution MRE acquisition and analysis protocol to reliably capture HCsf viscoelasticity. This MRE approach is the first to show differential age-related effects between HCsf viscoelasticity (Delgorio et al., 2021) and allows us to further explore individual HCsf mechanical structure-function relationships. One preliminary MRE study found relational memory performance to be specifically related to DG-CA3 viscoelasticity (Daugherty et al., 2020), suggesting that individual HCsf MRE measures may relate to different aspects of memory performance, though this preliminary work used imaging and inversion methods not optimized for examining the small HCsf. In this study, we use our higher resolution MRE approach to better capture the unique structure-function relationships in the HCsf across the lifespan, which may pave the way towards developing reliable clinical biomarkers related to cognitive decline in both aging and disease.

The purpose of this study is to determine how HCsf viscoelasticity supports different domains of memory, as quantified by performance on different cognitive tasks, by identifying if relationships exist between individual HCsf MRE measures and memory performance metrics. Based on previous studies, we hypothesize that CA1-CA2 viscoelasticity will associate with recall following an interference (Mueller et al., 2011; Molitor et al., 2021), SUB viscoelasticity will associate with delayed episodic recall (Travis et al., 2014; Zammit et al., 2017), and DG-CA3 viscoelasticity will relate to relational memory (Azab et al., 2014; Daugherty et al., 2020). Further, since both brain viscoelasticity and memory function change with age, we sought to evaluate if HCsf mechanical metrics may characterize the microstructural variation partially responsible for age-related differences in memory performance. We hypothesized that regional HCsf viscoelasticity mediates the relation between age and associated task performance.

Materials and Methods

Eighty-eight participants were included from three different studies (age range: 23-81 years, M/F: 36/51); all participants completed identical one-hour MRI scanning protocols on a 3T Siemens Prisma MRI scanner. Subsets of these data have been previously reported (Delgorio et al., 2021; Sanjana et al., 2021). We confirmed MRE data quality for each participant in our sample, as quantified by octahedral shear strain signal-to-noise ratio (OSS-SNR), and all 88 participants had OSS-SNR values greater than the threshold of 3.0 necessary for stable property estimation (McGarry et al., 2011; Hannum et al., 2021). Additionally, behavioral testing marginally differed between studies such that not every participant completed every cognitive task (see ‘Memory Assessment’ section below for more details).

<u>*High-Resolution MRE*</u>

Each MRI session included a high-resolution MRE acquisition and analysis protocol we recently developed for examining the HCsf (Figure 1) (Delgorio et al., 2021). A commercial Resoundant pneumatic driver (Resoundant, Rochester, MN) was used to apply 50 Hz acoustic vibrations and induce brain tissue deformation on the micron scale. A 3D multiband, multishot spiral MRE imaging sequence with 1.25 mm isotropic resolution was used to image the resulting deformations (240x240 mm^2 field-of-view, 192x192 imaging matrix, 96 slices, 1.25 mm slice thickness, TR/TE = 3360/70 ms) (Johnson et al., 2016a), which lasted approximately 10 minutes and 45 seconds. Structural scans included a T_1-weighted magnetization prepared rapid acquisition gradient echo (MPRAGE) scan at 0.9 mm isotropic resolution and a T_2-weighted turbo spin echo (TSE) scan with 0.4x0.4x2.0 mm^3 resolution aligned to the hippocampus, from which Automated Segmentation of Hippocampal Subfields (ASHS) segmented each HCsf region of interest: DG-CA3, CA1-CA2, and SUB (Yushkevich et al., 2015). FLIRT in FSL is used to transform the subfield segmentations into MRE space to create binary masks of each HCsf (Jenkinson et al., 2012). Finally, we used a nonlinear inversion algorithm (NLI) (McGarry et al., 2012) to calculate tissue property measures from displacement data using the HCsf as spatial priors through soft prior regularization (SPR) (McGarry et al., 2013). NLI is a finite-element based inversion method that accounts for the heterogeneous nature of tissue and produces reliable property images from data with sufficient OSS-SNR (McGarry et al., 2011). Reliability of local property estimations can be further improved by providing anatomical information using SPR (McGarry et al., 2013; Johnson et al., 2016b). NLI estimates the complex shear modulus ($G = G' + iG''$), where G' is the storage modulus and G'' is the loss modulus. which is used to compute the viscoelastic shear stiffness, $\mu = \frac{2|G|^2}{G'+|G|}$, and damping ratio, $\xi = \frac{G''}{2G'}$, that capture the effective stiffness and attenuation, respectively. To maximize sensitivity and repeatability of HCsf property estimates, we used NLI parameters optimized for HCsf with an SPR weighting of $\alpha = 10^{-12}$ and two different spatial filter widths: 0.9 mm for μ and 1.5 mm for ξ (Delgorio et al., 2021).

Figure 1 here

Memory Assessments

The memory battery included the California Verbal Learning Test III (CVLT) (Delis et al., 2017), Logical Memory (LM) from the Wechsler Memory Scale IV (Wechsler, 2009), and the spatial reconstruction (SR) task (Watson et al., 2013; Monti et al., 2014; Horecka et al., 2018). All participants completed the SR task (N = 88), while subsets of the participants also completed the CVLT (N = 73) and LM (N = 82) tasks.

California Verbal Learning Test: In the CVLT, the examiner read aloud a 16-word list (word list A) to participants a total of 5 times (i.e., trials). After each trial, participants recited the words they remembered back to the examiner. Participants were then read a second 16-word list (word list B) with semantically related items and were asked to recall as many of the words from this second word list that they could remember. Finally, participants asked to recall all the words they could remember from word list A. We calculated interference cost as the difference between recall of word list A, after the interference of word list B, and recall after the original fifth trial of word list A. Interference cost is an index of the loss of memory accuracy following mnemonic intrusions from semantically related items and has been associated with CA1-CA2 functional activation (Schlichting et al., 2014; Molitor et al., 2021). We also calculated delayed free recall score, which is the number of correct responses on word list A after a 30-minute delay.

Logical Memory: In the LM task, participants heard two short stories and were then asked to recall everything they remember immediately after the examiner recites each story and again after a delay period of 20-30 minutes. We calculated and analyzed the delayed free recall score as the sum of correct responses on recalling details from both story A and story B after the delay, which has previously been associated with SUB volumetric measures (Travis et al., 2014; Zammit et al., 2017).

Spatial Reconstruction: The SR task involved participants studying the locations of five abstract shapes for 20 seconds, which then disappear for four seconds and reappear at the top of the screen where participants are instructed to arrange the shapes based on how they remember the studied display (Watson et al., 2013; Monti et al., 2014). Performance on this task is determined by errors in object placement including displacements, edge resizing, rearrangement, and position swaps (Watson et al., 2013), from which we calculate the composite performance SR error score by combining standardized z-scores of each error metric; we have used the composite metric in our previous studies of MRE structure-function relationships (Schwarb et al., 2016, 2017; Daugherty et al., 2020). The SR error score was then converted (1 – SR error), such that higher numbers are indicative of better task performance. SR performance has previously been associated with DG-CA3 viscoelasticity (Daugherty et al., 2020), and relational memory and pattern separation have been related to DG- CA3 functional activation (Yassa et al., 2011; Azab et al., 2014).

<u>*Statistical Analysis*</u>

We computed sample mean, standard deviation, skew, and kurtosis for each MRE measure and behavioral outcome, and determined relationships between each variable, including bivariate correlations between each memory performance measure and stiffness, μ, and damping ratio, ξ, of each HCsf region. We detected outliers from the original raw datasets for both the memory task measures and HCsf MRE measures using a cutoff of 2.0x interquartile range (IQR). Outliers for each memory task measure were based on residuals from multiple regression models, with HCsf, age, and sex as predictors. Outliers for the HCsf regions were based on the mean distribution of the participant data. All outliers were removed for the relevant analyses accordingly.

Due to multicollinearity present among our predictors, ridge regression was used to investigate specific associations between the HCsf and each memory performance measure. Ridge regression is an extension of a multiple linear regression that addresses the problem of multicollinearity among independent variables, which is present in our HCsf MRE data (Daugherty et al., 2020; Delgorio et al., 2021). When independent variables are highly correlated to one another, parameters in linear regression become unstable (Daoud, 2018). Ridge regression addresses this issue by removing the unbiased estimate restriction that linear regression has, introducing a penalty term, 'k,' that decreases the size of the predictor variable coefficients. This in turn reduces model complexity and the overall effect of multicollinearity. This allows the model to consider the contribution of each independent predictor (i.e., HCsf region) more accurately (Golam Kibria, 2003). To confirm the presence of multicollinearity between the HCsf properties, we used multiple regression models to find the variance inflation factor (VIF) (Johnston et al., 2018).

We performed the ridge regression using R (v4.1.0) and the statistical package 'lmridge (v1.2)' (Ullah et al., 2018). For each memory measure, all HCsf regions were included as predictors of performance in one ridge regression model, with age and sex as additional predictor variables. We standardized the predictor variables and used the function 'kest' to determine the optimal 'k' based on the published literature. We chose the 'MED' equation for estimating 'k' (Golam Kibria, 2003) based on low mean square error and good performance on datasets with high variance and large sample sizes (Muniz and Kibria, 2009; Muniz et al., 2012; Najarian et al., 2013). For each ridge regression analysis, we considered the model R^2, which represents the cumulative variance explained by all the predictors in the model, and the individual coefficients, which represent the unique effect each predictor attributes to the model outcomes.

Finally, we sought to consider whether HCsf properties influence the relationship between age and memory performance, as both MRE properties and memory performance differ with age. We used mediation models to examine whether the relationship between age and memory performance may be mediated by HCsf μ and ξ, with one model tested for each memory measure and associated HCsf region relationship (as determined in the previous analysis). Mediation analyses were performed in Mplus (v8) (Muthén and Muthén, 2017); effect size and 95% confidence intervals not overlapping zero were interpreted as evidence of mediation (Hayes and Scharkow, 2013).

Results

Outliers were removed for CVLT (interference cost and delayed free recall; $n = 2$), SR ($n = 2$), and LM ($n = 4$) outcomes. Thus, our analyses were performed on the following final sample sizes: CVLT (N = 71); LM (N = 78); SR (N = 86). Table 1 describes an overview of the

MRE measurement demographics for all participants, with demographics for the memory task measures from the updated sample sizes without outliers.

Table 1 here

Correlations between HCsf, Memory, Age, and Sex

Bivariate correlations between the individual HCsf μ and ξ properties revealed the HCsf were highly correlated with one another ($r > 0.7$). Additionally, all HCsf were significantly related to age for both μ ($r > -0.47$) and ξ ($r > 0.47$). The relationship between sex and both DG-CA3 and CA1-CA2 μ displayed small effect sizes ($d = 0.20$ and 0.36, respectively), while the SUB μ and sex relationship displayed a moderate effect size ($d = 0.56$). Similarly, the relationship between sex and all HCsf ξ displayed small effect sizes ($d < 0.50$) (Table 2). However, sex was included as a factor in analyses as MRE studies have shown sexual dimorphism in brain mechanical properties and potentially different relationships with age between males and females (Sack et al., 2009; Arani et al., 2015; Hiscox et al., 2020b). From all multiple regression models, the VIF for DG-CA3 μ, CA1-CA2 μ, and all HCsf ξ were greater than the threshold of 2.5 indicating multicollinearity, while the VIF of SUB μ was 2.2 and close to the threshold (Johnston et al., 2018).

Table 2 here

Figure 2 shows correlations between μ of each HCsf region and performance on each memory task, without controlling for age and sex. Each HCsf region μ (DG-CA3, CA1-CA2, and SUB) correlated significantly with performance on memory tasks CVLT interference cost, LM delayed free recall, and SR (all $p < 0.05$), with higher HCsf μ associating with better memory performance, while only DG-CA3 μ correlated significantly with CVLT delayed free recall. Figure 3 shows correlations between ξ of each HCsf region and performance on each memory task, without controlling for age and sex. No significant correlations were present between HCsf region ξ (DG-CA3, CA1-CA2, and SUB) and performance on CVLT interference cost, CVLT delayed free recall, and LM delayed free recall ($p > 0.05$). For SR performance, all HCsf ξ were significantly correlated ($p < 0.01$), with lower HCsf ξ associating with better memory performance. Specific p and r values for each structure-function relationship are indicated on each plot in Figures 2 and 3.

Figure 2 here

Figure 3 here

Age was also significantly related to CVLT interference cost performance ($r = -0.24$, $p = 0.042$), CVLT delayed free recall performance ($r = -0.37$, $p = 0.002$), LM delayed free recall performance ($r = -0.34$, $p = 0.002$), and SR performance ($r = -0.66$, $p < 0.001$). Sex did not display large effect sizes for any memory task measure ($d < 0.43$). Figures 4 and 5 display the age correlations with all memory measures (Figure 4) and HCsf MRE measures (Figure 5).

Figure 4 here

Figure 5 here

HCsf Structure-Function Relationships

For each memory task measure, all HCsf regions were included as predictors in a ridge regression model, along with age and sex. Table 3 presents a summary of the ridge regression results for each stiffness-memory model, while Table 4 presents a summary of the ridge regression results for each damping ratio-memory model. Each model description for both Tables 3 and 4 included (1) the total model R^2 and (2) the individual predictor ridge estimators ('b') and if they were significant in relation to the entire model. Statistically significant ridge estimators indicate that specific predictors contributed a significantly larger effect to the overall model variance compared to the other predictors.

Stiffness-memory ridge regression models: The optimal 'k' value for the CVLT interference cost ridge regression model was 2.38. The overall R^2 was 0.033 and CA1-CA2 μ was the only subfield region that significantly predicted task performance ($b = 0.90$, $p = 0.018$). No other subfield was significant in the model ($p > 0.05$). The optimal 'k' value for CVLT delayed free recall was 0.15. The overall R^2 was 0.169 and no HCsf μ were significant contributors of CVLT delayed free recall performance, though age ($b = -10.1$, 0.002) and sex ($b = 7.58$, $p = 0.010$) were both significant contributors. The optimal 'k' value for the LM delayed free recall model was 0.89. The overall R^2 was 0.098 and both DG-CA3 μ ($b = 6.14$, $p = 0.016$) and SUB μ ($b = 5.73$, $p = 0.032$) were the only significant predictors of delayed free recall performance. The optimal 'k' value for the SR model was 0.072. The overall R^2 was 0.415 and CA1-CA2 μ was the only significant subfield predictor of SR performance ($b = 2.32$, $p = 0.011$), while the other subfield regions were not significant predictors ($p > 0.05$). Additionally, age was a strong predictor of SR performance ($b = -4.17$, $p < 0.001$).

<u>Table 3 here</u>

Damping ratio-memory ridge regression models: For all models, no HCsf region significantly predicted any memory performance measure ($p > 0.1$). However, age was a significant contributor to CVLT delayed free recall performance ($b = -9.67$, $p < 0.001$), LM delayed free recall performance ($b = -7.36$, $p = 0.005$), and SR performance ($b = -3.90$, $p < 0.001$). Sex was also a significant contributor to CVLT delayed free recall performance ($b = 5.73$, $p = 0.017$).

Table 4 here

We also considered individual HCsf volume as predictors of memory task performance as HCsf volume is a common measure of tissue integrity and can be related to MRE measures of tissue integrity. All HCsf volumes were corrected for head size (intracranial volume, ICV) using the analysis of covariance (ANCOVA) approach, which corrects regional measures based on the proportion of the difference between an individual's ICV and the average ICV for the sample (Jack et al., 1989). Indeed, both DG-CA3 and CA1-CA2 exhibit significant correlations between μ and volume ($p < 0.05$), but not SUB, while no HCsf exhibited significant correlations between ξ and volume (Table 5).

Table 5 here

For each ridge regression models we included volume of each HCsf as predictors in addition to HCsf μ, age, and sex, as before. Including these additional predictors did not change the outcomes with μ of previously identified HCsf being the only significant predictors: CVLT interference cost and CA1-CA2 μ ($p = 0.030$); LM delayed free recall and DG-CA3 μ (p =

0.009) and SUB μ (p = 0.016); and SR and CA-CA2 μ (p = 0.009). Table 6 presents complete ridge regression results from the model including volume.

Table 6 here

HCsf Stiffness as a Mediator of Age Effects on Memory Performance

Based on the results from the ridge regression analyses, we performed individual mediation models for each memory task to assess whether the individual HCsf stiffness influenced the relationship between age and memory performance. Mediation models were performed for each of the statistically significant HCsf stiffness-memory task relationships: CA1-CA2 μ and CVLT interference cost, DG-CA3 μ and SUB μ and LM delayed free recall, and CA1-CA2 μ and SR. Figure 6 illustrates the results for each model, including direct relationships between each variable and the indirect mediated effect. CA1-CA2 μ significantly mediates the effect of age on CVLT performance (*indirect* = -0.15, p = 0.031, 95% confidence interval (CI) [-0.30, -0.02]), accounting for 62.4% of the total effect of age on performance. The LM mediation model revealed that both DG-CA3 μ *(indirect* = -0.13, p = 0.050, 95% CI [-0.27, -0.01]) and SUB μ (*indirect* = -0.13, p = 0.054, 95% CI [-0.27, -0.01]) have 95% CI that do not overlap zero, supporting mediation that accounts for 39.8% and 39.5% of the total age effect explained by DG-CA3 μ and SUB μ, respectively. However, it should be noted these effect sizes are moderate and did not reach statistical significance. For the SR task, the model indicated that CA1-CA2 μ did not mediate the relationship between age and performance *(indirect* = -0.099, p = 0.073, 95% CI [-0.21, 0.01]), accounting for only 15.1% of the total age effect.

Figure 6 here

Discussion

Our goal was to identify if hypothesized unique associations existed between HCsf viscoelasticity and specific memory domains across the adult lifespan. These results agree with previous studies showing that while all HCsf are integral to good memory performance, each region uniquely contributes to specific aspects of declarative memory encoding, recall, and retrieval (Zeineh et al., 2003; Lee et al., 2004; Dimsdale-Zucker et al., 2018), which can be observed with MRE. Our results complement previous MRE findings of strong structure-function correlations between HC viscoelasticity and memory (Schwarb et al., 2016), as well as dissociable relationships with other structures and functions, such as frontal cortex with fluid intelligence and rule learning (Johnson et al., 2018; Schwarb et al., 2019). Our high-resolution MRE approach allows us to identify structure-function dissociations between the small neighboring HCsf for the first time, confirming the sensitivity of MRE measures to relevant microstructural integrity in these regions, including that individual HCsf μ measures appear to be stronger predictors of memory than volume measures.

We focused on three mnemonic processes associated with hippocampal function: interference, delayed episodic recall, and relational memory. Previous volumetry and functional MRI work has indicated that interference cost on traditional memory tasks is associated with CA1-CA2 structure (Mueller et al., 2011; Molitor et al., 2021). Consistent with these findings, we showed that CA1-CA2 μ was the strongest predictor for two types of memory performance: recall following an interference and short-delay relational memory. CA1-CA2 is often associated with delayed recall and memory consolidation (Mueller et al., 2011; Zammit et al., 2017). Some studies suggest CA1 has a role in integrating related events with overlapping neural representation, such as two similar word lists (Molitor et al., 2021) and match/mismatch detection (Duncan et al., 2012; Schlichting et al., 2014). Additionally, prior work revealed gradual, linear changes in CA1 activation when recalling semantically-related items or words with increasing similarity (Leal and Yassa, 2018). Interference cost from the CVLT is a measure of recall performance of a rehearsed list of words following presentation of an interference list, which is consistent with the ability to detect differences between semantically-related items (Kane and Engle, 2000), and thus supports the correlation with CA1-CA2 μ we observe here. Prior imaging studies in older adults and dementia patients displayed similar correlations between CA1 volume and delayed verbal recall (Kerchner et al., 2012; Zammit et al., 2017), including CVLT delayed recall performance in cognitively impaired older adults (Mueller et al., 2011). While interference cost is determined from immediate recall, there is potentially overlap in strategies for both immediate and delayed recall on this task. Overall, the role of CA1 in encoding and differentiating between related events as well as verbal recall performance support the significant contribution of CA1-CA2 μ to resolving interference in memory recall.

Significant associations between SUB μ and LM task performance support prior work that shows delayed episodic recall performance is associated with SUB volumetry (Travis et al., 2014; Zammit et al., 2017). SUB is related to integrating and projecting information onto the greater extra-hippocampal regions (O'Mara et al., 2009; Newmark et al., 2013; Travis et al., 2014). Prior *in vivo* research showed associations between SUB volume and verbal free recall (Hartopp et al., 2019), showcasing the important role of the SUB in recall after a delay. From the tasks in this study, delayed episodic recall is also a standard measure for the CVLT; however, there were no significant associations between CVLT delayed free recall and any HCsf μ measure in the ridge regression analysis. These non-significant results are likely due to lack of variability in the task measurement range for the sample, with most participants recalling many words correctly.

Additionally, both functional MRI and MRE studies have shown that associative or relational memory measures are related to DG-CA3 (Azab et al., 2014; Daugherty et al., 2020). Relational memory is the ability to bind arbitrary information into a single representation (Cohen and Eichenbaum, 1995; Eichenbaum and Cohen, 2004), which is critical to remembering story details required in the LM task through deep encoding strategies to create associations among details from the stories for recall after the delay (Wechsler, 2009). This is consistent with our results showing LM performance was related to DG-CA3 μ. Neural signals from the DG-CA3 to the SUB are conveyed via the tri-synaptic circuit (Duvernoy, 2005), and thus both structures have a role in memory encoding. Specifically, DG-CA3 is thought to support associative memory function and is related to encoding and subsequent recall of bound information (Berron et al., 2016; Hainmueller and Bartos, 2020; Bouyeure et al., 2021).

Surprisingly, DG-CA3 μ was not associated with SR performance. SR is a relational memory task (Monti et al., 2014; Horecka et al., 2018) that has been correlated with DG-CA3 viscoelastic measures in a young adult sample (Daugherty et al., 2020). In the current study, SR performance was uniquely associated instead with CA1-CA2 μ and a smaller, non-significant unique effect of DG-CA3. Age-related differences in CA1-CA2 structure are commonly reported to be larger than in DG-CA3 (Daugherty et al., 2016), and the vulnerability of CA1-CA2 in aging may account for its larger unique effect on SR performance here. SR requires encoding from multiple objects and locations, as well as detecting errors when the participant places objects during the reconstruction phase of the task (Watson et al., 2013; Monti et al., 2014; Horecka et al., 2018). Therefore, the task plausibly requires the synchronous function of CA1 and DG-CA3 within the tri-synaptic circuit, where the DG granule and CA3 pyramidal cells signal and transfer information to the CA1 pyramidal cells (Duvernoy, 2005). Indeed, strategies for completing this task can engage similar processes as reflected by CVLT interference cost. For instance, participants visually navigate the space with strategic viewing patterns that influence later reconstruction performance on this task (Lucas et al., 2018); thus, potentially influencing the firing rates observed in CA1-CA2. In pre-surgical epilepsy patients, differences between CA1 and dorsolateral prefrontal cortex gamma power (an index of network activity) predicted the precision of spatial memory judgments (Stevenson et al., 2018), which further supports relational memory functions of CA1-CA2.

Aging affects both HCsf integrity and memory performance, and as such, examining age-related differences can shed light on structure-function relationships in the brain. Our group previously demonstrated that aging strongly affects HCsf viscoelasticity, and with differential effects between HCsf (Delgorio et al., 2021). Thus, we also investigated the role of HCsf viscoelasticity to partially account for age-related differences in memory performance. Of the significant HCsf structure-function relationships observed in the ridge analysis, we found evidence of CA1-CA2 μ strongly mediating the effect of age on CVLT performance, and moderate effect sizes of both DG-CA3 μ and SUB μ mediating the effect on LM performance. Overall, these results indicate that low HCsf μ contributes to worse memory performance with age, which is consistent with previous findings using diffusion MRI methods (Hayek et al., 2020; Radhakrishnan et al., 2020). Our data is cross-sectional, so our results from the mediation models must be cautiously interpreted (Lindenberger et al., 2011), but these findings motivate future longitudinal analyses.

There were several additional limitations present in our study. Relationships between HCsf structure and function were observed with μ, but not ξ, despite previous studies reporting relationships between memory performance and HC ξ, but not μ (Schwarb et al., 2016, 2017, 2019; Daugherty et al., 2020; Hiscox et al., 2020a). The reasons for this discrepancy are not immediately clear, however, previous reports all studied narrow age ranges of either young or older adults, while some included only male participants. This work included both male and female adult participants across a large age range of 60 years. Examining our current sample using subsets of participants in similar age ranges as those studies (i.e. < 35 years or > 65 years), we did not observe any significant correlations between either HCsf μ or ξ and memory task outcomes in either group, though these subsamples are smaller and less powered to detect such effects, and a future study designed to understand how these structure-function relationships may change across the lifespan is warranted. We note that in recent studies on pediatric participants, MRE structure-function relationships were observed in μ but not ξ (McIlvain et al., 2020a, 2020b). We also recognize that this study shows weaker evidence of structure-function dissociations than in our prior MRE work that reported a double dissociation in structure-function relationships of relational memory and fluid intelligence performance with viscoelasticity of the HC and orbitofrontal cortex (Johnson et al., 2018). This is due to the memory functions examined here each depending on the HC as whole, in addition to being particularly supported by individual HCsf, making dissociations more difficult to observe.

Here, we show through MRE metrics that the HCsf regions uniquely contribute to specific memory task domains. These qualities make MRE a promising tool to track prodromal neuropathology, improving differential diagnosis of dementia subtypes in the future. Future studies will involve classifying similar structure-function relationships in patients with Alzheimer's disease and mild cognitive impairment.

References

Arani A, Murphy MC, Glaser KJ, Manduca A, Lake DS, Kruse S, Jack Jr CR, Ehman R, Huston J (2015) Measuring the effects of aging and sex on regional brain stiffness with MR elastography in healthy older adults. NeuroImage 111:59–64.

Azab M, Stark SM, Stark CEL (2014) Contributions of human hippocampal subfields to spatial and temporal pattern separation. Hippocampus 24:293–302.

Berron D, Schütze H, Maass A, Cardenas-Blanco A, Kuijf HJ, Kumaran D, Düzel E (2016) Strong evidence for pattern separation in human dentate gyrus. Journal of Neuroscience 36:7569–7579.

Bouyeure A, Patil S, Mauconduit F, Poiret C, Isai D, Noulhiane M (2021) Hippocampal subfield volumes and memory discrimination in the developing brain. Hippocampus 31:1202–1214.

Cohen NJ, Eichenbaum H (1995) Memory, amnesia, and the hippocampal system. MIT press.

Daoud JI (2018) Multicollinearity and Regression Analysis. In: Journal of Physics: Conference Series. Institute of Physics Publishing.

Daugherty AM, Bender AR, Raz N, Ofen N (2016) Age differences in hippocampal subfield volumes from childhood to late adulthood. Hippocampus 26:220–228.

Daugherty AM, Schwarb HD, McGarry MDJ, Johnson CL, Cohen NJ (2020) Magnetic Resonance Elastography of Human Hippocampal Subfields: CA3-Dentate Gyrus Viscoelasticity Predicts Relational Memory Accuracy. Journal of Cognitive Neuroscience 32:1704–1713.

de Flores R, la Joie R, Chételat G (2015) Structural imaging of hippocampal subfields in healthy aging and Alzheimer's disease. Neuroscience 309:29–50.

Delgorio PL, Hiscox LV, Daugherty AM, Sanjana F, Pohlig RT, Ellison JM, Martens CR, Schwarb H, McGarry MDJ, Johnson CL (2021) Effect of Aging on the Viscoelastic Properties of Hippocampal Subfields Assessed with High-Resolution MR Elastography. Cerebral Cortex 31:2799–2811.

Delis DC, Kramer JH, Kaplan E, Ober BA (2017) The California Verbal Learning Test-3 (3rd ed.). Psychological Corporation.

Dimsdale-Zucker HR, Ritchey M, Ekstrom AD, Yonelinas AP, Ranganath C (2018) CA1 and CA3 differentially support spontaneous retrieval of episodic contexts within human hippocampal subfields. Nature Communications 9:1–8.

Duncan K, Ketz N, Inati SJ, Davachi L (2012) Evidence for area CA1 as a match/mismatch detector: A high-resolution fMRI study of the human hippocampus. Hippocampus 22:389–398.

Duvernoy HM (2005) The human hippocampus: functional anatomy, vascularization and serial sections with MRI. Springer Science & Business Media.

Eichenbaum H, Cohen NJ (2004) From conditioning to conscious recollection: Memory systems of the brain. Oxford University Press on Demand.

Foster CM, Kennedy KM, Hoagey DA, Rodrigue KM (2019) The role of hippocampal subfield volume and fornix microstructure in episodic memory across the lifespan. Hippocampus 29:1206–1223.

Golam Kibria BM (2003) Performance of some New Ridge regression estimators. Communications in Statistics Part B: Simulation and Computation 32:419–435.

Golomb J, Kluger A, de Leon MJ, Ferris SH, Mittelman MP, Cohen J, George AE (1996) Hippocampal formation size predicts declining memory performance in normal aging. Neurology 47:810–813.

Hainmueller T, Bartos M (2020) Dentate gyrus circuits for encoding, retrieval and discrimination of episodic memories. Nature Reviews Neuroscience 21:153–168.

Hannum AJ, McIlvain G, Sowinski D, McGarry MDJ, Johnson CL (2021) Correlated noise in brain magnetic resonance elastography. Magnetic Resonance in Medicine 87:1313–1328.

Hartopp N, Wright P, Ray NJ, Evans TE, Metzler-Baddeley C, Aggleton JP, O'Sullivan MJ (2019) A key role for subiculum-fornix connectivity in recollection in older age. Frontiers in Systems Neuroscience 12:70.

Hayek D, Thams F, Flöel A, Antonenko D (2020) Dentate Gyrus Volume Mediates the Effect of Fornix Microstructure on Memory Formation in Older Adults. Frontiers in Aging Neuroscience 12:79.

Hayes AF, Scharkow M (2013) The relative trustworthiness of inferential tests of the indirect effect in statistical mediation analysis: does method really matter? Psychol Sci 24:1918–1927.

Hiscox LV, Johnson CL, Barnhill E, McGarry MDJ, Huston J, van Beek EJR, Starr JM, Roberts N (2016) Magnetic resonance elastography (MRE) of the human brain: Technique, findings and clinical applications. Physics in Medicine and Biology 61:R401–R437.

Hiscox LV, Johnson CL, McGarry MDJ, Perrins M, Littlejohn A, van Beek EJR, Roberts N, Starr JM (2018) High-resolution magnetic resonance elastography reveals differences in subcortical gray matter viscoelasticity between young and healthy older adults. Neurobiology of Aging 65:158–167.

Hiscox LV, Johnson CL, McGarry MDJ, Schwarb H, van Beek EJR, Roberts N, Starr JM (2020a) Hippocampal viscoelasticity and episodic memory performance in healthy older adults examined with magnetic resonance elastography. Brain Imaging Behav 14:175–185.

Hiscox LV, McGarry MDJ, Schwarb H, van Houten EEW, Pohlig RT, Roberts N, Huesmann GR, Burzynska AZ, Sutton BP, Hillman CH, Kramer AF, Cohen NJ, Barbey AK, Paulsen KD, Johnson CL (2020b) Standard-space atlas of the viscoelastic properties of the human brain. Human Brain Mapping 41:5282–5300.

Hiscox LV, Schwarb H, McGarry MDJ, Johnson CL (2021) Aging brain mechanics: Progress and promise of magnetic resonance elastography. NeuroImage 232:117889.

Horecka KM, Dulas MR, Schwarb H, Lucas HD, Duff M, Cohen NJ (2018) Reconstructing relational information. Hippocampus 28:164–177.

Jack CR, Twomey CK, Zinsmeister AR, Sharbrough FW, Petersen RC, Cascino GD, Fws N (1989) Anterior temporal lobes and hippocampal formations: normative volumetric measurements from MR images in young adults. Radiology 172:549–554.

Jenkinson M, Beckmann CF, Behrens TEJ, Woolrich MW, Smith SM (2012) Fsl. NeuroImage 62:782–790.

Johnson CL, Holtrop JL, Anderson AT, Sutton BP (2016a) Brain MR elastography with multiband excitation and nonlinear motion-induced phase error correction. In: Proceedings of the 24th Annual Meeting of the International Society for Magnetic Resonance in Medicine, pp 1951.

Johnson CL, Schwarb H, Horecka KM, McGarry MDJ, Hillman CH, Kramer AF, Cohen NJ, Barbey AK (2018) Double dissociation of structure-function relationships in memory and fluid intelligence observed with magnetic resonance elastography. NeuroImage 171:99–106.

Johnson CL, Schwarb H, McGarry MDJ, Anderson AT, Huesmann GR, Sutton BP, Cohen NJ (2016b) Viscoelasticity of subcortical gray matter structures. Human Brain Mapping 37:4221–4233.

Johnston R, Jones K, Manley D (2018) Confounding and collinearity in regression analysis: a cautionary tale and an alternative procedure, illustrated by studies of British voting behaviour. Quality and Quantity 52:1957–1976.

Kane MJ, Engle RW (2000) Working-memory capacity, proactive interference, and divided attention: limits on long-term memory retrieval. Journal of Experimental Psychology: Learning, Memory, and Cognition 26:336.

Kerchner GA, Deutsch GK, Zeineh M, Dougherty RF, Saranathan M, Rutt BK (2012) Hippocampal CA1 apical neuropil atrophy and memory performance in Alzheimer's disease. NeuroImage 63:194–202.

Leal SL, Yassa MA (2018) Integrating new findings and examining clinical applications of pattern separation. Nature Neuroscience 21:163–173.

Lee I, Rao G, Knierim JJ (2004) A Double Dissociation between Hippocampal Subfields: Differential Time Course of CA3 and CA1 Place Cells for Processing Changed Environments. Neuron 42:803–815.

Lindenberger U, von Oertzen T, Ghisletta P, Hertzog C (2011) Cross-Sectional Age Variance Extraction: What's Change Got To Do With It? Psychology and Aging 26:34–47.

Lucas HD, Duff MC, Cohen NJ (2018) The hippocampus promotes effective saccadic information gathering in humans. Journal of Cognitive Neuroscience 31:186–201.

McGarry MDJ, Johnson CL, Sutton BP, van Houten EEW, Georgiadis JG, Weaver JB, Paulsen KD (2013) Including spatial information in nonlinear inversion MR elastography using soft prior regularization. IEEE Trans Med Imaging 32:1901–1909.

McGarry MDJ, van Houten EEW, Johnson CL, Georgiadis JG, Sutton BP, Weaver JB, Paulsen KD (2012) Multiresolution MR elastography using nonlinear inversion. Medical Physics 39:6388–6396.

McGarry MDJ, van Houten EEW, Perrinez PR, Pattison AJ, Weaver JB, Paulsen KD (2011) An octahedral shear strain-based measure of SNR for 3D MR elastography. Physics in Medicine & Biology 56:N153.

McIlvain G, Clements RG, Magoon EM, Spielberg JM, Telzer EH, Johnson CL (2020a) Viscoelasticity of reward and control systems in adolescent risk taking. NeuroImage 215:116850.

McIlvain G, Tracy JB, Chaze CA, Petersen DA, Villermaux GM, Wright HG, Miller F, Crenshaw JR, Johnson CL (2020b) Brain Stiffness Relates to Dynamic Balance Reactions in Children With Cerebral Palsy. Journal of Child Neurology 35:463–471.

Molitor RJ, Sherril KR, Morton NW, Miller AA, Preston AR (2021) Memory reactivation during learning simultaneously promotes dentate gyrus/CA2, 3 pattern differentiation and CA1 memory integration. Journal of Neuroscience 41:726–738.

Monti JM, Cooke GE, Watson PD, Voss MW, Kramer AF, Cohen NJ (2014) Relating hippocampus to relational memory processing across domains and delays. J Cogn Neurosci 27:234–245.

Morrison JH, Hof PR (1997) Life and death of neurons in the aging brain. Science (1979) 278:412–419.

Mueller SG, Chao LL, Berman B, Weiner MW (2011) Evidence for functional specialization of hippocampal subfields detected by MR subfield volumetry on high resolution images at 4T. NeuroImage 56:851–857.

Mueller SG, Stables L, Du AT, Schuff N, Truran D, Cashdollar N, Weiner MW (2007) Measurement of hippocampal subfields and age-related changes with high resolution MRI at 4 T. Neurobiology of Aging 28:719–726.

Muniz G, Kibria BM, Shukur G (2012) On Developing Ridge Regression Parameters: A Graphical Investigation. Department of Mathematics and Statistics 10 Available at: https://digitalcommons.fiu.edu/math_fac/10.

Muniz G, Kibria BMG (2009) On some ridge regression estimators: An empirical comparisons. Communications in Statistics: Simulation and Computation 38:621–630.

Murphy MC, Huston J, Ehman RL (2019) MR elastography of the brain and its application in neurological diseases. NeuroImage 187:176–183.

Muthén B, Muthén L (2017) Mplus. Chapman and Hall/CRC.

Najarian S, Arashi M, Kibria BMG (2013) A simulation study on some restricted ridge regression estimators. Communications in Statistics: Simulation and Computation 42:871–890.

Newmark RE, Schon K, Ross RS, Stern CE (2013) Contributions of the hippocampal subfields and entorhinal cortex to disambiguation during working memory. Hippocampus 23:467–475.

O’Mara SM, Sanchez-Vives MV, Brotons-Mas JR, O’Hare E (2009) Roles for the subiculum in spatial information processing, memory, motivation and the temporal control of behaviour. Progress in Neuro-Psychopharmacology and Biological Psychiatry 33:782–790.

Petersen RC, Jack CR, Xu Y-C, Waring SC, O’brien PC, Smith GE, Ivnik RJ, Tangalos EG, Boeve BF, Kokmen E (2000) Memory and MRI-based hippocampal volumes in aging and AD. Neurology 54:581.

Radhakrishnan H, Stark SM, Stark CEL (2020) Microstructural Alterations in Hippocampal Subfields Mediate Age-Related Memory Decline in Humans. Frontiers in Aging Neuroscience 12:94.

Sack I, Beierbach B, Wuerfel J, Klatt D, Hamhaber U, Papazoglou S, Martus P, Braun J (2009) The impact of aging and gender on brain viscoelasticity. NeuroImage 46:652–657.

Sack I, Jöhrens K, Würfel J, Braun J (2013) Structure-sensitive elastography: On the viscoelastic powerlaw behavior of in vivo human tissue in health and disease. Soft Matter 9:5672–5680.

Sanjana F, Delgorio PL, Hiscox LV, DeConne TM, Hobson JC, Cohen ML, Johnson CL, Martens CR (2021) Blood lipid markers are associated with hippocampal viscoelastic properties and memory in humans. Journal of Cerebral Blood Flow and Metabolism 41:1417–1427.

Schlichting ML, Zeithamova D, Preston AR (2014) CA1 subfield contributions to memory integration and inference. Hippocampus 24:1248–1260.

Schwarb H, Johnson CL, Daugherty AM, Hillman CH, Kramer AF, Cohen NJ, Barbey AK (2017) Aerobic fitness, hippocampal viscoelasticity, and relational memory performance. NeuroImage 153:179–188.

Schwarb H, Johnson CL, Dulas MR, McGarry MDJ, Holtrop JL, Watson PD, Wang JX, Voss JL, Sutton BP, Cohen NJ (2019) Structural and Functional MRI Evidence for Distinct Medial Temporal and Prefrontal Roles in Context-dependent Relational Memory. J Cogn Neurosci 31:1857–1872.

Schwarb H, Johnson CL, McGarry MDJ, Cohen NJ (2016) Medial temporal lobe viscoelasticity and relational memory performance. NeuroImage 132:534–541.

Stevenson RF, Zheng J, Mnatsakanyan L, Vadera S, Knight RT, Lin JJ, Yassa MA (2018) Hippocampal CA1 gamma power predicts the precision of spatial memory judgments. Proc Natl Acad Sci U S A 115:10148–10153.

Travis SG, Huang Y, Fujiwara E, Radomski A, Olsen F, Carter R, Seres P, Malykhin N v. (2014) High field structural MRI reveals specific episodic memory correlates in the subfields of the hippocampus. Neuropsychologia 53:233–245.

Ullah MI, Aslam M, Altaf S (2018) lmridge: A Comprehensive R Package for Ridge Regression. R J 10:326.

Watson PD, Voss JL, Warren DE, Tranel D, Cohen NJ (2013) Spatial reconstruction by patients with hippocampal damage is dominated by relational memory errors. Hippocampus 23:570–580.

Wechsler D (2009) WMS-IV: Wechsler memory scale. Pearson.

West MJ (1993) Regionally specific loss of neurons in the aging human hippocampus. Neurobiol Aging 14:287–293.

Wisse LEM, Biessels GJ, Heringa SM, Kuijf HJ, Luijten PR, Geerlings MI, Group UVCIVCIS (2014) Hippocampal subfield volumes at 7T in early Alzheimer’s disease and normal aging. Neurobiol Aging 35:2039–2045.

Yassa MA, Lacy JW, Stark SM, Albert MS, Gallagher M, Stark CEL (2011) Pattern separation deficits associated with increased hippocampal CA3 and dentate gyrus activity in nondemented older adults. Hippocampus 21:968–979.

Yushkevich PA, Pluta JB, Wang H, Xie L, Ding SL, Gertje EC, Mancuso L, Kliot D, Das SR, Wolk DA (2015) Automated volumetry and regional thickness analysis of hippocampal subfields and medial temporal cortical structures in mild cognitive impairment. Human Brain Mapping 36:258–287.

Zammit AR, Ezzati A, Zimmerman ME, Lipton RB, Lipton ML, Katz MJ (2017) Roles of hippocampal subfields in verbal and visual episodic memory. Behavioural Brain Research 317:157–162.

Zeineh MM, Engel SA, Thompson PM, Bookheimer SY (2003) Dynamics of the Hippocampus During Encoding and Retrieval of Face-Name Pairs. Science (1979) 299:577–580.

Data Availability

Data is available upon request.

Figure Legends

Figure 1: Overview of the HCsf-specific high-resolution MRE protocol. (A) In step one, we applied 50 Hz micron-level vibrations with a Resoundant pneumatic actuator via a passive head pillow driver. (B) In step two, we used a 1.25mm isotropic resolution multiband, multishot MRE sequence to image the shear waves generated in (A). (C) In steps three and four, we first used ASHS to segment the HCsf regions of interest (DG-CA3, CA1-CA2, and SUB) and then used NLI to generate measurements of shear stiffness for each HCsf region (Delgorio et al., 2021).

Figure 2: Overview of simple bivariate correlations between HCsf regional μ and memory performance measures (not correcting for age and sex). Correlations observed between each HCsf region and CVLT III interference cost performance (A-C) and delayed free recall performance (D-F). Correlations observed between each HCsf region and logical memory delayed free recall performance (G-I). Correlations observed between each HCsf region and SR performance (J-L). (* $p < 0.05$; ** $p < 0.01$; *** $p < 0.001$).

Figure 3: Overview of simple bivariate correlations between HCsf regional ξ and memory performance measures (not correcting for age and sex). Correlations observed between each HCsf region and CVLT III interference cost performance (A-C) and delayed free recall performance (D-F). Correlations observed between each HCsf region and logical memory

delayed free recall performance (G-I). Correlations observed between each HCsf region and SR performance (J-L). (* $p < 0.01$; ** $p < 0.001$).

Figure 4: Summary of bivariate correlations between memory measures and age. (A) CVLT interference cost performance and age were significantly related ($r = -0.24$, $p = 0.042$). (B) CVLT delayed free recall performance and age were significantly related ($r = -0.37$, $p = 0.002$). (C) LM delayed free recall performance and age were significantly related ($r = -0.34$, $p = 0.002$). (D) SR performance and age were significantly related ($r = -0.66$, $p < 0.001$).

Figure 5: Summary of bivariate correlations between HCsf MRE measures and age. (A-C) Bivariate correlations between HCsf μ and age. All regions were significantly related to age ($p < 0.001$). (D-F) Bivariate correlations between HCsf ξ and age. All regions were significantly related to age ($p < 0.01$).

Figure 6: Mediation results for all memory task models. (A) **CVLT:** CA1-CA2 μ significantly mediates the relationship between age and interference cost (indirect = -0.15, $p = 0.031$). (B and C) **Logical Memory:** Both DG-CA3 μ (indirect = -0.13, $p = 0.050$) and SUB μ (indirect = -0.13, $p = 0.054$) models have 95% CI that do not overlap zero, supporting mediation, although the effect sizes do not reach statistical significance. Together this indicates DG-CA3 μ and SUB μ may have a moderate influence on logical memory performance across the lifespan. (D) **Spatial Reconstruction:** CA1-CA2 μ does not mediate the effect of age on SR (indirect = -0.099, $p = 0.073$) in this sample.

Tables

Table 1: Participant Demographics and Distribution of MRE and Memory Outcome Measures

Category	Measure	Mean (SD)	Min/Max	|S|	|K|
Demographics	Age (years)	59.7 (15.8)	23.0/81.0	-1.12	0.23
MRE μ (kPa)	DG-CA3	3.21 (0.45)	1.63/4.20	-0.63	1.10
	CA1-CA2	3.28 (0.42)	1.89/4.24	-0.35	0.38
	SUB	2.97 (0.46)	1.73/4.03	-0.39	-0.16
MRE ξ	DG-CA3	0.21 (0.04)	0.14/0.30	0.43	-0.03
	CA1-CA2	0.19 (0.03)	0.12/0.27	0.08	-0.60
	SUB	0.15 (0.04)	0.09/0.24	0.58	-0.40
Memory Tasks	*CVLT III*: Interference Cost	-1.49 (1.67)	-6.00/2.00	-0.44	0.01
	CVLT III: Delayed Free Recall	11.4 (3.54)	1.0/16.0	-0.62	-0.06
	Logical Memory: Delayed Free Recall	24.7 (5.95)	12.0/40.0	0.15	-0.17
	Spatial Reconstruction	0.06 (0.84)	-1.69/1.43	-0.32	-0.75

|S|: skewness, |K|: kurtosis, < or > 1.96 for |S| and |K| indicate a violation of the assumption of normality

Table 1: Overview of the participant demographics, including sample age distribution, MRE μ and ξ distribution for all HCsf regions, and memory task distribution for each task.

Table 2: Summary of Bivariate Correlation Coefficients for all HCsf Regional MRE measures, Age, and Sex

Bivariate Correlations for HCsf μ			
	DG-CA3 μ	**CA1-CA2 μ**	**SUB μ**
DG-CA3 μ	-		
CA1-CA2 μ	0.86*	-	
SUB μ	0.71*	0.74*	-
Age	-0.47*	-0.56*	-0.51*
Sex†	0.20	0.36	0.56
Bivariate Correlations for HCsf ξ			
	DG-CA3 ξ	**CA1-CA2 ξ**	**SUB ξ**
DG-CA3 ξ	-		
CA1-CA2 ξ	0.89*	-	
SUB ξ	0.83*	0.87*	-
Age	0.47*	0.58*	0.52*
Sex†	0.25	0.43	0.50

** p < 0.001*
† This row contains Cohen's d effect sizes

Table 2: Summary of bivariate correlations between all HCsf regional MRE measures, age, and sex. Correlations between the HCsf μ showed that all regions were significantly correlated to one another ($p < 0.001$). Additionally, all HCsf μ were also significantly related to age ($p < 0.001$). There were small effect sizes in the relationships between sex and DG-CA3 ($d = 0.20$) and CA1-CA2 μ ($d = 0.36$), while the relationship between sex and SUB μ displayed a medium effect size ($d = 0.56$). Correlations between the HCsf ξ showed that all regions were significantly correlated to one another ($p < 0.001$). Additionally, all HCsf ξ were also significantly related to age ($p < 0.001$). There were small effect sizes in the relationships between sex and all HCsf ξ ($d < 0.5$).

Table 3: Overview of the ridge regression results for each memory task model, including HCsf μ. b and p-values are given for each predictor variable.

	CVLT III: Interference Cost		CVLT III: Delayed Free Recall		Logical Memory: Delayed Free Recall		Spatial Reconstruction	
R^2	0.033		0.169		0.098		0.415	
k-value	2.376		0.150		0.888		0.072	
Results	**b-weight**	**p-value**	**b-weight**	**p-value**	**b-weight**	**p-value**	**b-weight**	**p-value**
Age	-0.66	0.135	**-10.1**	**0.002****	-5.26	0.065	**-4.17**	**< 0.001*****
Sex	0.01	0.984	**7.58**	**0.010***	0.58	0.842	0.55	0.362
DG-CA3 μ	0.74	0.055	3.66	0.293	**6.14**	**0.016***	-0.69	0.423
CA1-CA2 μ	**0.90**	**0.018***	-2.11	0.550	2.82	0.239	**2.32**	**0.011***
SUB μ	0.67	0.10	0.76	0.823	**5.73**	**0.032***	-0.51	0.516

** p < 0.05, ** p < 0.01, *** p < 0.001*

Table 3: Overview of the ridge regression results for each memory task, HCsf μ model. **CVLT Interference Cost:** CA1-CA2 μ was the only significant HCsf predictor of interference cost performance (b = 0.90, p = 0.018). **CVLT Delayed Free Recall:** There were no significant HCsf μ predictors of CVLT delayed free recall performance. Age (b = -10.1, p = 0.002) and sex (b = 7.58, p = 0.010) were the only significant predictors of task performance. **Logical Memory:** Both DG-CA3 μ (b = 6.14, p = 0.016) and SUB μ (b = 5.73, p = 0.032) were significant HCsf predictors of logical memory delayed free recall performance. **Spatial Reconstruction:** CA1-CA2 μ was the only significant HCsf predictor of spatial reconstruction performance (b = 2.32, p = 0.011). Age was also a significant predictor for this task (b = -4.17, p < 0.001).

Table 4: Overview of the ridge regression results for each memory task model, including HCsf ξ. b and p-values are given for each predictor variable.

	CVLT III: Interference Cost		CVLT III: Delayed Free Recall		Logical Memory: Delayed Free Recall		Spatial Reconstruction	
R^2	0.031		0.102		0.047		0.231	
k-value	0.996		0.377		0.811		0.211	
Results	**b-weight**	**p-value**	**b-weight**	**p-value**	**b-weight**	**p-value**	**b-weight**	**p-value**
Age	-1.31	0.104	**-9.67**	**< 0.001*****	**-7.36**	**0.005****	**-3.90**	**< 0.001*****
Sex	0.04	0.962	**5.73**	**0.017***	-0.57	0.832	0.46	0.401
DG-CA3 ξ	-0.44	0.502	0.15	0.948	-1.73	0.401	0.38	0.528
CA1-CA2 ξ	-0.47	0.417	0.58	0.775	1.28	0.488	-0.85	0.147
SUB ξ	-0.62	0.349	1.62	0.478	-1.41	0.498	-0.28	0.655

** p < 0.05, ** p < 0.01, *** p < 0.001*

Table 4: Overview of the ridge regression results for each memory task, HCsf ξ model. **CVLT Interference Cost:** There were no significant HCsf ξ predictors of CVLT interference cost performance. **CVLT Delayed Free Recall:** There were no significant HCsf ξ predictors of CVLT delayed free recall performance. Age (b = -9.67, p < 0.001) and sex (b = 5.73, p = 0.017) were the only significant predictors of task performance. **Logical Memory:** There were no significant HCsf ξ predictors of logical memory delayed free recall performance. Age was the only significant predictor of logical memory delayed free recall performance (b = -7.36, p = 0.005). **Spatial Reconstruction:** There were no significant HCsf ξ predictors of spatial reconstruction performance. Age was the only significant predictor of logical memory delayed free recall performance (b = -3.90, p < 0.001).

Table 5: Correlations between HCsf MRE measures, μ and ξ, with HCsf volume.

	DG-CA3	CA1-CA2	SUB
μ vs. volume	0.36***	0.51***	0.05
ξ vs. volume	-0.13	-0.17	0.004

*** *p < 0.001*

Table 5: Summary of bivariate correlations between all HCsf regional MRE measures, μ and ξ, with HCsf volume. Correlations between the HCsf μ and volume measures showed that both DG-CA3 and CA1-CA2 μ were significantly correlated with DG-CA3 and CA1-CA2 volume, respectively ($p < 0.001$). SUB μ and volume were not significantly correlated ($p > 0.6$). Correlations between the HCsf ξ and volume measures showed that all regions were not significantly correlated to one another ($p > 0.1$).

Table 6: Overview of the ridge regression results for each memory task model, including both HCsf μ and volume. b and p-values are given for each predictor variable.

	CVLT III: Interference Cost		CVLT III: Delayed Free Recall		Logical Memory: Delayed Free Recall		Spatial Reconstruction	
R^2	0.062		0.102		0.097		0.303	
k-value	0.973		0.565		1.18		0.417	
Results	**b-weight**	**p-value**	**b-weight**	**p-value**	**b-weight**	**p-value**	**b-weight**	**p-value**
Age	-0.92	0.232	**-6.40**	**0.003****	-4.24	0.071	**-2.81**	**< 0.001*****
Sex	0.06	0.944	**5.06**	**0.016***	0.705	0.774	0.391	0.394
DG-CA3 μ	0.963	0.153	2.29	0.220	**5.51**	**0.009****	0.059	0.892
CA1-CA2 μ	**1.38**	**0.030***	0.164	0.926	2.06	0.278	**1.11**	**0.009****
SUB μ	0.842	0.239	0.629	0.746	**5.35**	**0.016***	0.156	0.732
DG-CA3 volume	0.206	0.774	2.51	0.200	-1.73	0.427	-0.007	0.988
CA1-CA2 volume	-0.035	0.959	-1.17	0.533	3.24	0.123	0.761	0.086
SUB volume	-0.565	0.475	-1.30	0.529	4.08	0.092	0.553	0.231

** p < 0.05, ** p < 0.01, *** p < 0.001*

Table 6: Overview of the ridge regression results for each memory task, HCsf μ model, including HCsf volume. **CVLT Interference Cost:** CA1-CA2 μ was the only significant HCsf predictor of interference cost performance (b = 1.38, p = 0.030). There were no significant HCsf volume predictors of interference cost performance. **CVLT Delayed Free Recall:** There were no significant HCsf μ and volume predictors of CVLT delayed free recall performance. Age (b = -6.40, p = 0.003) and sex (b = 5.06, p = 0.016) were the only significant predictors of task performance. **Logical Memory:** Both DG-CA3 μ (b = 5.51, p = 0.009) and SUB μ (b = 5.35, p = 0.016) were significant HCsf predictors of logical memory delayed free recall performance. There were no significant HCsf volume predictors of logical memory delayed free recall performance **Spatial Reconstruction:** CA1-CA2 μ was the only significant HCsf predictor of spatial reconstruction performance (b = 1.11, p = 0.009). Age was also a significant predictor for this task (b = -2.81, p < 0.001). There were no significant HCsf volume predictors of spatial reconstruction performance.

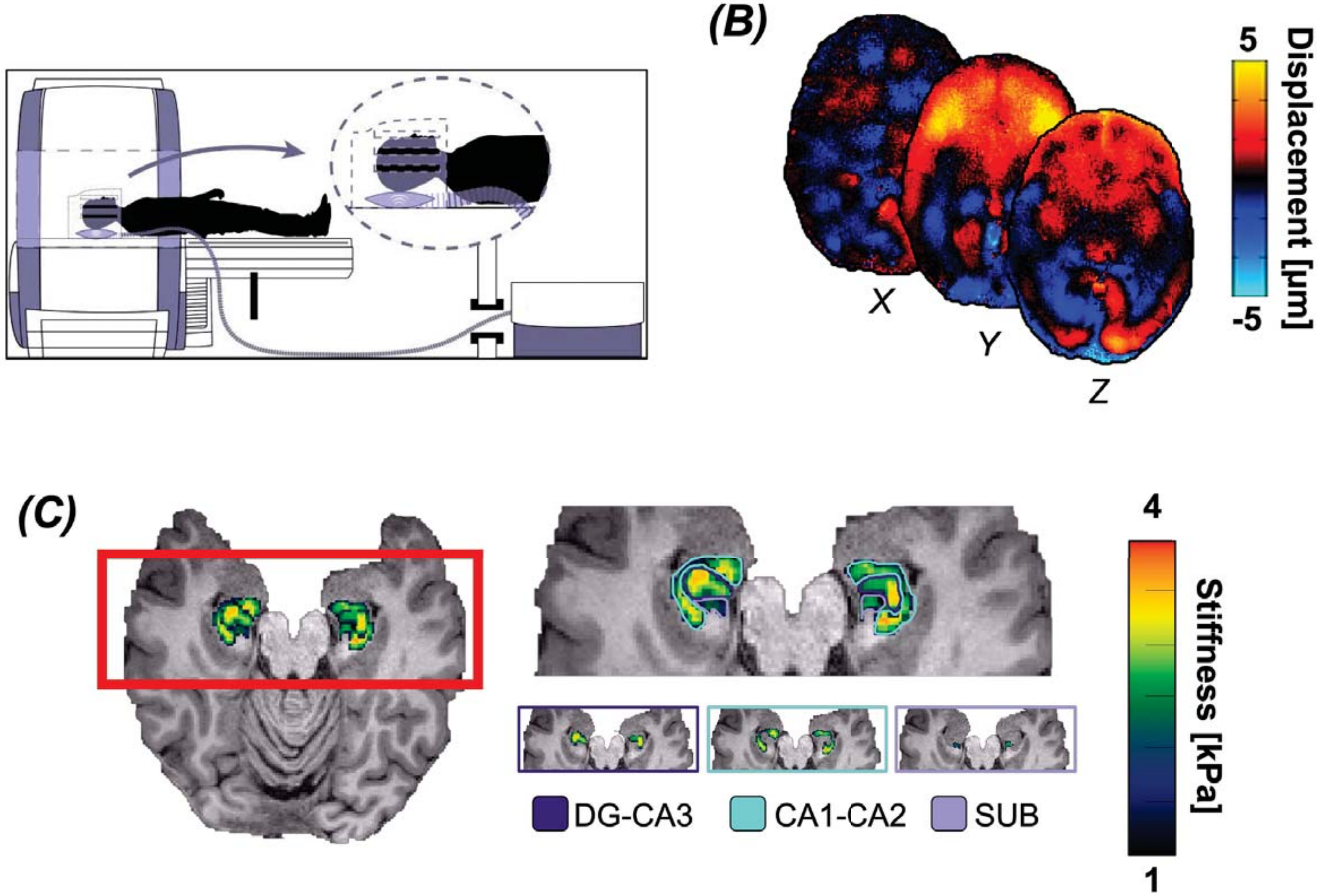

(A)
(B)
X
Y
Z
5
-5
Displacement [µm]
(C)
DG-CA3
CA1-CA2
SUB
4
1
Stiffness [kPa]

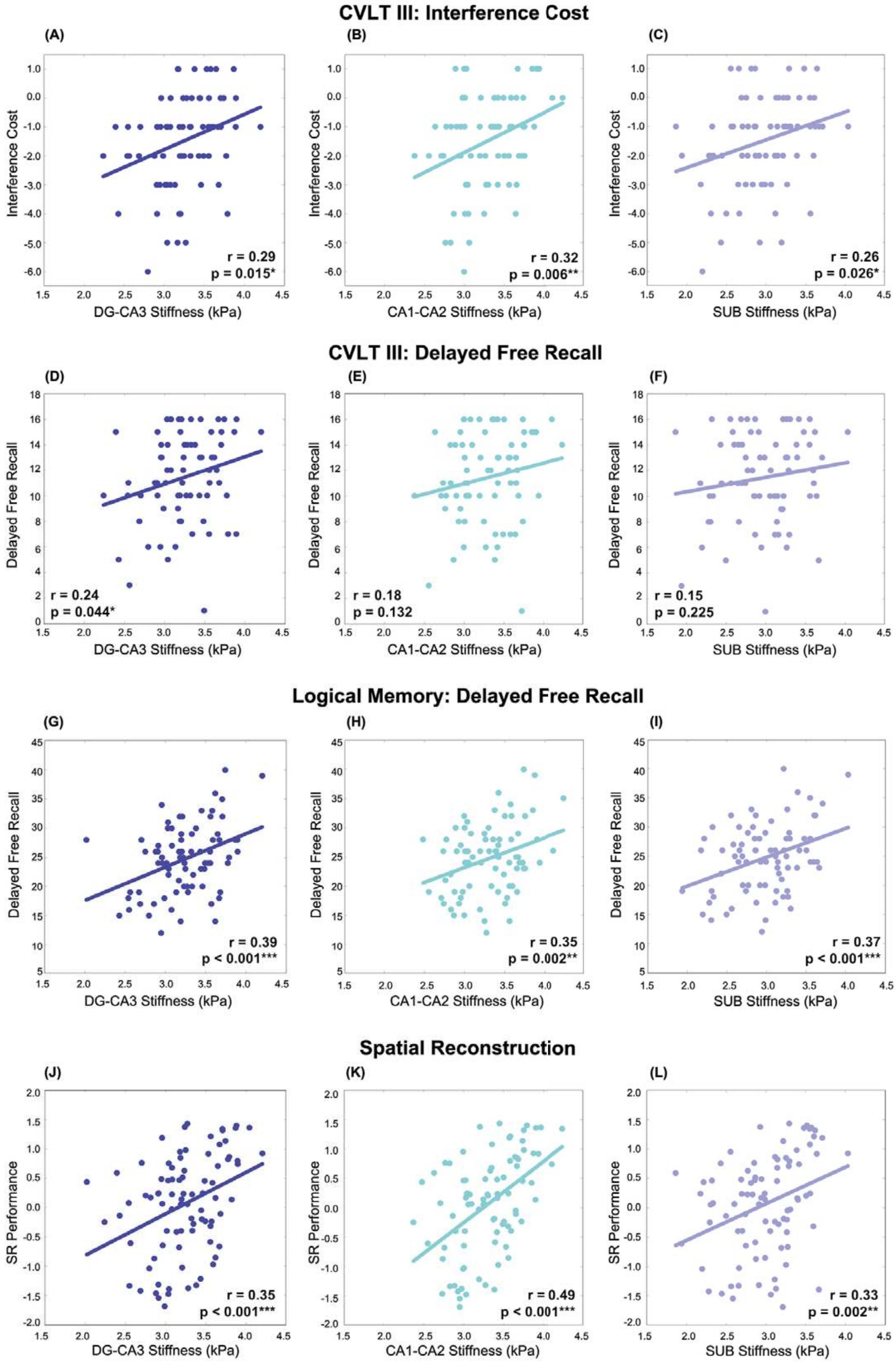
CVLT III: Interference Cost
(A)
Interference Cost
DG-CA3 Stiffness (kPa)
r = 0.29
p = 0.015*
(B)
Interference Cost
CA1-CA2 Stiffness (kPa)
r = 0.32
p = 0.006**
(C)
Interference Cost
SUB Stiffness (kPa)
r = 0.26
p = 0.026*
CVLT III: Delayed Free Recall
(D)
Delayed Free Recall
DG-CA3 Stiffness (kPa)
r = 0.24
p = 0.044*
(E)
Delayed Free Recall
CA1-CA2 Stiffness (kPa)
r = 0.18
p = 0.132
(F)
Delayed Free Recall
SUB Stiffness (kPa)
r = 0.15
p = 0.225
Logical Memory: Delayed Free Recall
(G)
Delayed Free Recall
DG-CA3 Stiffness (kPa)
r = 0.39
p < 0.001***
(H)
Delayed Free Recall
CA1-CA2 Stiffness (kPa)
r = 0.35
p = 0.002**
(I)
Delayed Free Recall
SUB Stiffness (kPa)
r = 0.37
p < 0.001***
Spatial Reconstruction
(J)
SR Performance
DG-CA3 Stiffness (kPa)
r = 0.35
p < 0.001***
(K)
SR Performance
CA1-CA2 Stiffness (kPa)
r = 0.49
p < 0.001***
(L)
SR Performance
SUB Stiffness (kPa)
r = 0.33
p = 0.002**

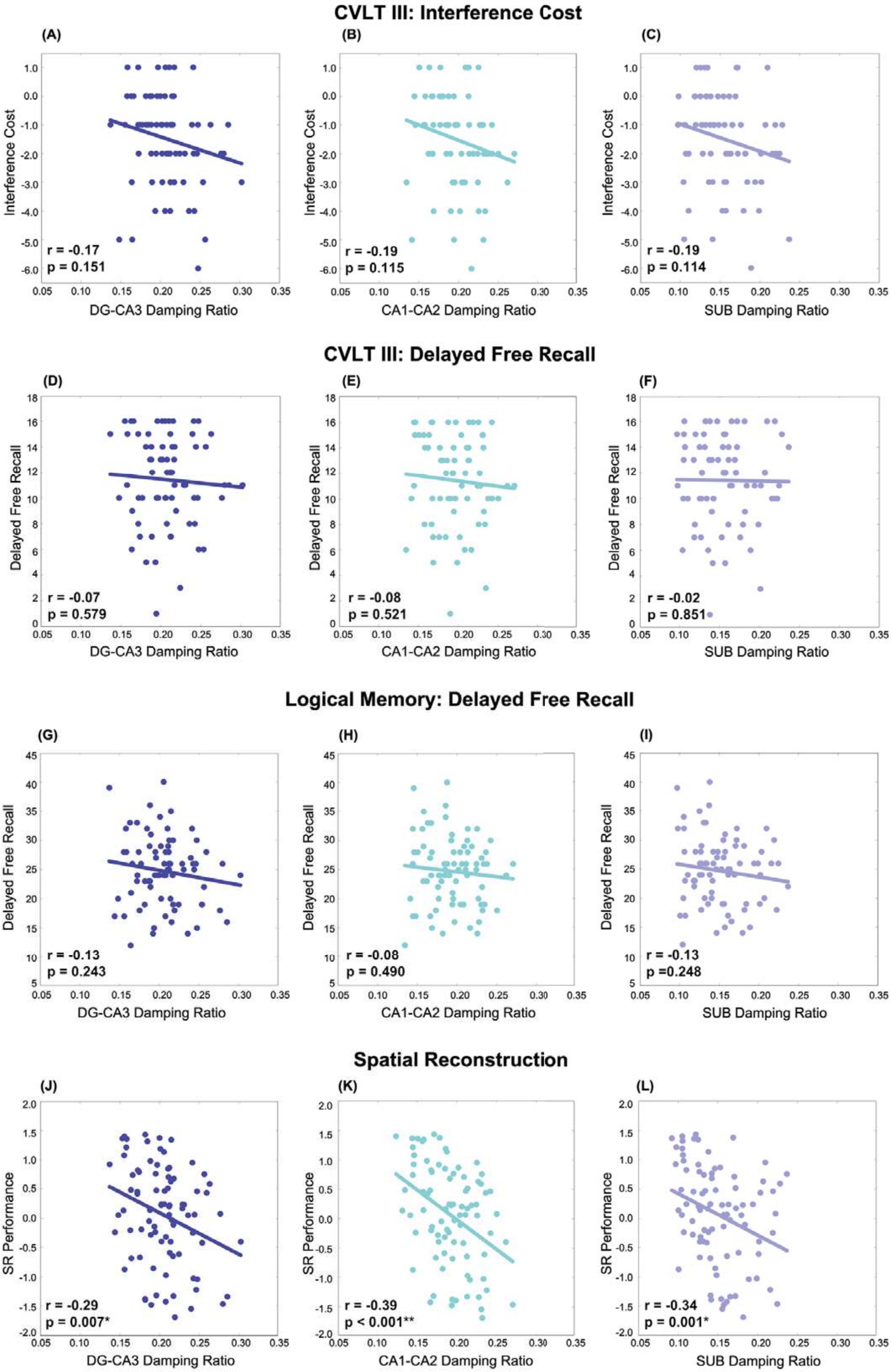
CVLT III: Interference Cost
(A)
Interference Cost
r = -0.17
p = 0.151
DG-CA3 Damping Ratio
(B)
Interference Cost
r = -0.19
p = 0.115
CA1-CA2 Damping Ratio
(C)
Interference Cost
r = -0.19
p = 0.114
SUB Damping Ratio
CVLT III: Delayed Free Recall
(D)
Delayed Free Recall
r = -0.07
p = 0.579
DG-CA3 Damping Ratio
(E)
Delayed Free Recall
r = -0.08
p = 0.521
CA1-CA2 Damping Ratio
(F)
Delayed Free Recall
r = -0.02
p = 0.851
SUB Damping Ratio
Logical Memory: Delayed Free Recall
(G)
Delayed Free Recall
r = -0.13
p = 0.243
DG-CA3 Damping Ratio
(H)
Delayed Free Recall
r = -0.08
p = 0.490
CA1-CA2 Damping Ratio
(I)
Delayed Free Recall
r = -0.13
p =0.248
SUB Damping Ratio
Spatial Reconstruction
(J)
SR Performance
r = -0.29
p = 0.007*
DG-CA3 Damping Ratio
(K)
SR Performance
r = -0.39
p < 0.001**
CA1-CA2 Damping Ratio
(L)
SR Performance
r = -0.34
p = 0.001*
SUB Damping Ratio

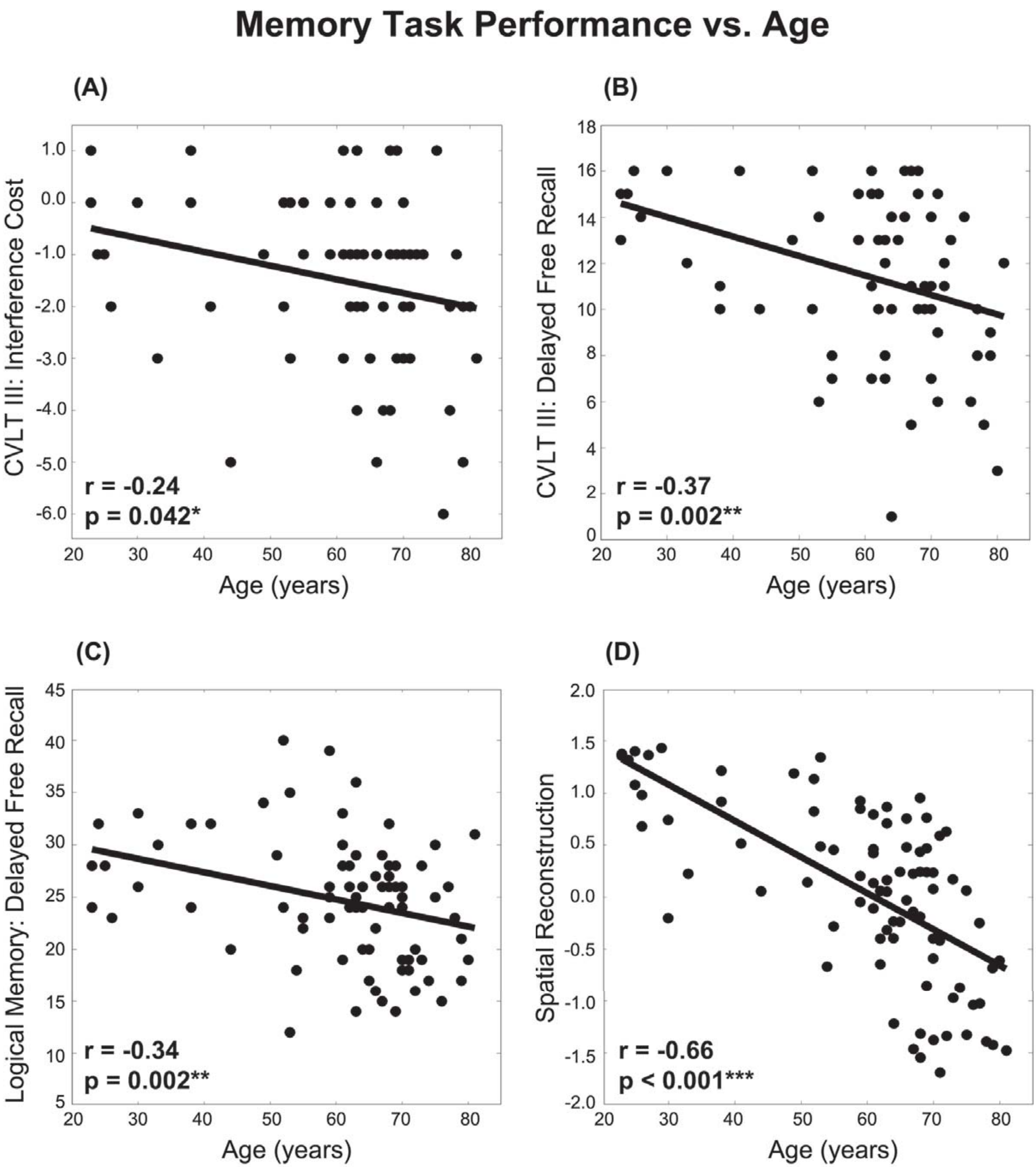
Memory Task Performance vs. Age
(A)
CVLT III: Interference Cost
r = -0.24
p = 0.042*
Age (years)
(B)
CVLT III: Delayed Free Recall
r = -0.37
p = 0.002**
Age (years)
(C)
Logical Memory: Delayed Free Recall
r = -0.34
p = 0.002**
Age (years)
(D)
Spatial Reconstruction
r = -0.66
p < 0.001***
Age (years)

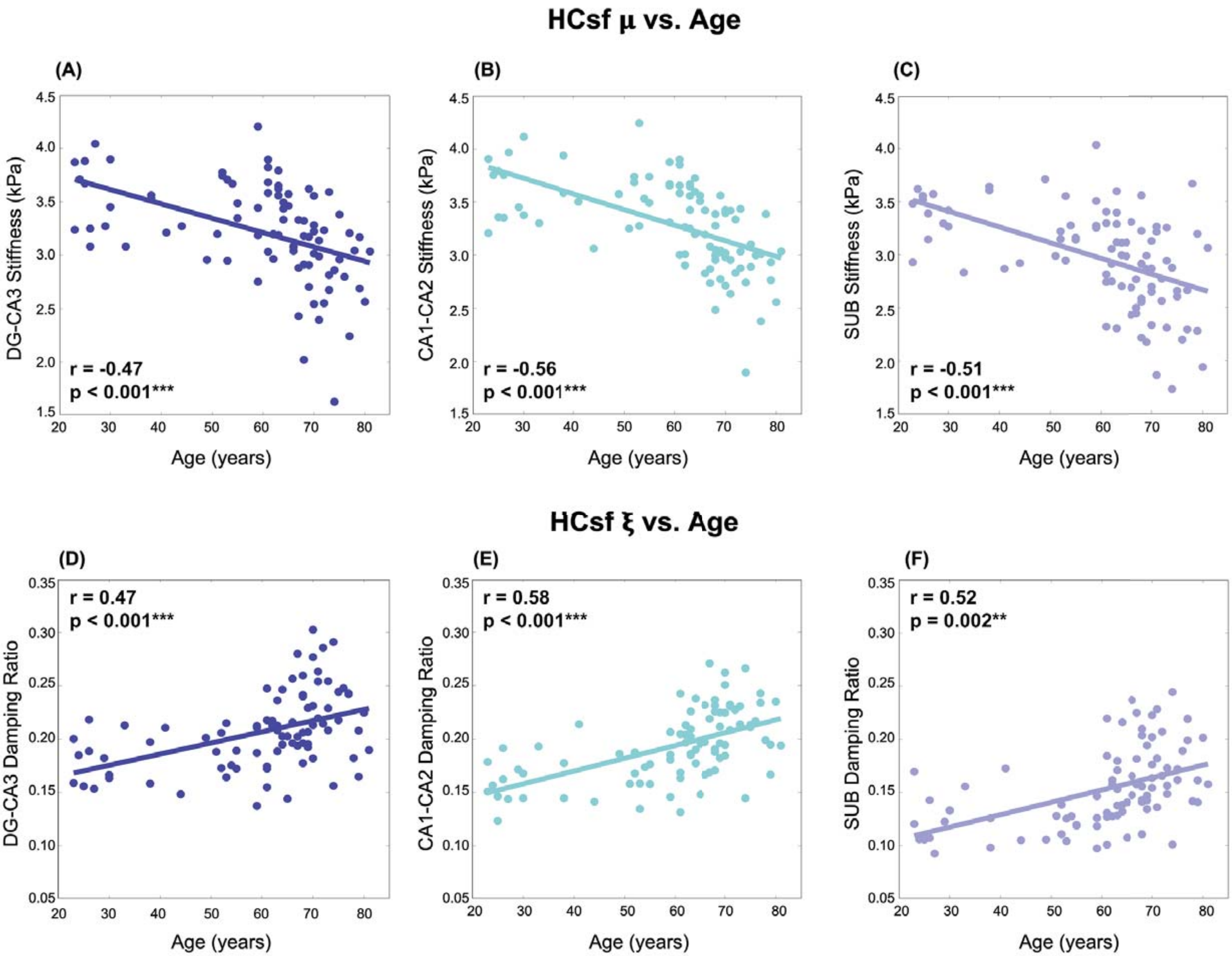
HCsf μ vs. Age
(A)
DG-CA3 Stiffness (kPa)
r = -0.47
p < 0.001***
Age (years)
(B)
CA1-CA2 Stiffness (kPa)
r = -0.56
p < 0.001***
Age (years)
(C)
SUB Stiffness (kPa)
r = -0.51
p < 0.001***
Age (years)
HCsf ξ vs. Age
(D)
DG-CA3 Damping Ratio
r = 0.47
p < 0.001***
Age (years)
(E)
CA1-CA2 Damping Ratio
r = 0.58
p < 0.001***
Age (years)
(F)
SUB Damping Ratio
r = 0.52
p = 0.002**
Age (years)

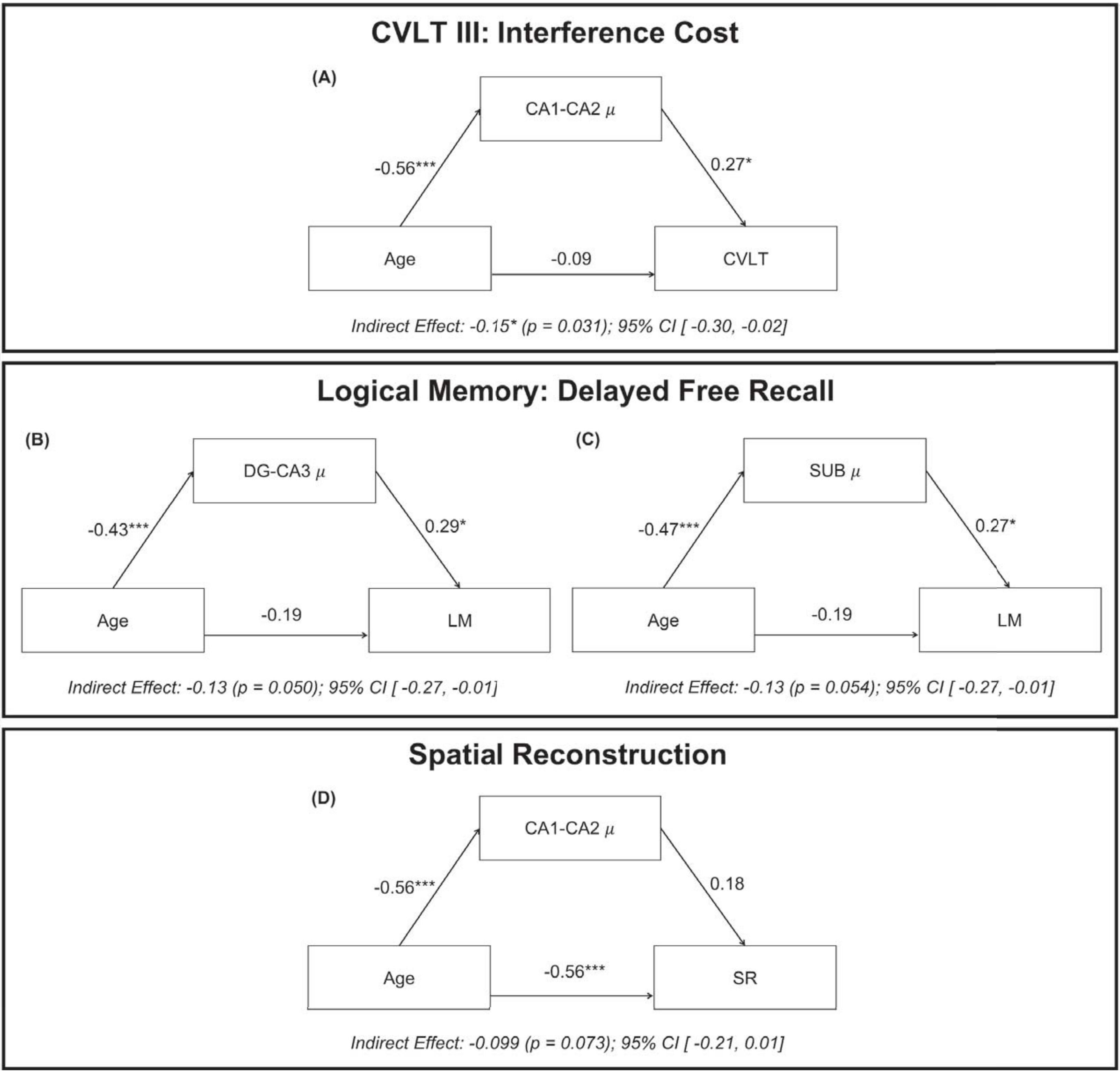
CVLT III: Interference Cost
(A)
CA1-CA2 μ
-0.56***
0.27*
Age
-0.09
CVLT
Indirect Effect: -0.15* (p = 0.031); 95% CI [-0.30, -0.02]
Logical Memory: Delayed Free Recall
(B)
DG-CA3 μ
-0.43***
0.29*
Age
-0.19
LM
Indirect Effect: -0.13 (p = 0.050); 95% CI [-0.27, -0.01]
(C)
SUB μ
-0.47***
0.27*
Age
-0.19
LM
Indirect Effect: -0.13 (p = 0.054); 95% CI [-0.27, -0.01]
Spatial Reconstruction
(D)
CA1-CA2 μ
-0.56***
0.18
Age
-0.56***
SR
Indirect Effect: -0.099 (p = 0.073); 95% CI [-0.21, 0.01]